Available online at www.sciencedirect.com
SCIENCE DIRECT
Journal of Molecular Catalysis A: Chemical 242 (2005) 182–194
JOURNAL OF MOLECULAR CATALYSIS A: CHEMICAL
www.elsevier.com/locate/molcata

Hydrogen evolution on nickel incorporated in three-dimensional conducting polymer layers

Elisa Navarro-Flores, Sasha Omanovic *

Department of Chemical Engineering and McGill Institute for Advanced Materials, McGill University, 3610 University Street, Montreal, Que., Canada H3A 2B2

Received 21 June 2005; received in revised form 5 August 2005; accepted 5 August 2005
Available online 9 September 2005

Abstract

The paper discusses results on the development of nickel/conducting polymer composite layers used as catalysts in the hydrogen evolution reaction (HER). Conducting polymers (CP), polypyrrole (PPY), and polyaniline (PANI) are used as three-dimensional pattering templates (matrices) for electrodeposition of nickel on an inert glassy carbon surface. It is shown that Ni/CP layers offer a significantly higher overall electrocatalytic activity in the HER than Ni electrodeposited on a flat two-dimensional substrate. This is a result of favorable Ni/CP morphology which yields an increase in the active surface area of the catalyst.

The overall best catalyst is a Ni/PANI layer formed by incorporation of small amounts of Ni into a thick pre-deposited PANI layer. The resulting porous layer is composed of ca. 3 μm interconnected spherical Ni particles, with an almost complete surface absence of PANI. The increased porosity of the layer is of a great benefit at high HER overpotentials, where accumulation of produced molecular hydrogen inside the catalyst layer is prevented. Due to a lower porosity, all the Ni/PPY catalytic layers studied are susceptible to the surface blockage (hydrogen accumulation) at high overpotentials. However, in the lower overpotential region, a Ni/PPY catalyst formed by incorporating a larger amount of Ni into a thin porous pre-deposited PPY layer offers an electrocatalytic HER activity comparable to the best Ni/PANI catalyst. When PPY and Ni are electrodeposited simultaneously (co-deposition method), a substantial decrease in a diameter of Ni islands, down to 100 nm, and an increase in the island surface density are obtained.

Keywords: Hydrogen; Water electrolysis; Electrocatalysis; Nickel; Conducting polymers; Polypyrrole; Polyaniline

1. Introduction

One of the major problems of today's world is in its heavy dependency on fossil fuels, which, in turn, creates a range of socio-economical, geopolitical, and environmental problems. The utilization of fossil fuels, especially oil, is predicted to increase exponentially in the coming years, while at the same time their availability will decrease. This will contribute to a further increase of the above problems. However, it has already been obvious that the solution to these problems is to increase the use of sustainable energy resources. Since hydrogen, the most abundant element on earth, is the cleanest and ideal fuel (carrier), it has been increasingly considered as the *fuel of the future* [1–4]. Although production of hydrogen by water electrolysis is not currently cost-competitive to natural gas reforming, it represents a process where hydrogen can be produced by true renewable and fully environmentally friendly energy sources (solar, wind, and hydro), without co-production of the green-house gas, CO_2. Industrial water electrolysis is, for the time, being carried out using a liquid alkaline electrolyte. The disadvantages of this technology are mainly related to low specific production rates, high energy consumption, low efficiency, voluminous systems, and safety issues related to use of caustic electrolytes. However, the use of solid polymer electrolyte membrane (PEM)-type generators (the technology very similar to the PEM fuel cell technology) with demineralized water as the raw material would offer a viable alternative to the alkaline process, especially for residential and small-scale applications. Although the inherent advantages of the PEM technology over the alkaline one are clearly established (greater safety and reli-

* Corresponding author. Tel.: +1 514 398 4273; fax: +1 514 398 6678.
E-mail address: sasha.omanovic@mcgill.ca (S. Omanovic).

1381-1169/$ – see front matter © 2005 Elsevier B.V. All rights reserved.
doi:10.1016/j.molcata.2005.08.008

ability, higher differential pressures, higher operating current densities and efficiency, rapid transient responses, construction simplicity, maintenance, etc.), one of the main obstacles associated with the large-scale commercial application of the PEM hydrogen generator is related to high investment costs. This is mainly due to the use of noble metals (Pt, Ir, and Ru) as electroactive catalyst materials [5,6]. It has been recently shown [7] that the major portion of the cost of the hydrogen infrastructure based on the use of wind turbines (in Germany) is related to the hydrogen generator (water electrolyser). In the same study, the authors have shown that the cost of the hydrogen gas produced by wind-powered water electrolysis and used to fuel a passenger car is still twice the cost of diesel fuel in Germany (normalize with respect to the mileage). However, due to the rapidly increasing cost of the oil, the authors predict that the situation will become opposite in the near future. Therefore, there is a great need to develop a more active, efficient, stable, and cheap electrocatalysts for water splitting in the PEM hydrogen generator that would offer low overpotentials for the hydrogen evolution reaction (HER) at rather high current densities (1–2 A cm^{-2}), and ultimately lower the cost of produced hydrogen.

Three properties play an important role in selecting catalytically active materials for the HER: (a) an actual *intrinsic* electrocatalytic effect of the material, (b) a large active surface area per unit volume ratio, both of which are directly related to the (over)potential used to operate the electrolyzer at significant current densities, and (c) catalyst stability. Consequently, an approach used in the design of good HER electrocatalysts is based either on the increase of the active surface area of the electrode (catalyst) [8–11] and/or on the design of an electrode material of a high intrinsic catalytic activity [12–16]. We have previously shown [17] that by alloying nickel with left transition metals (W, Mo, and Fe), an increase in the intrinsic electrocatalytic activity in the HER, compared to pure nickel, can be obtained. Although NiW has been shown to offer the highest intrinsic activity, NiMo has yielded the highest overall activity. This is mainly due to the favorable catalyst's morphology (high surface roughness). In general, the research on the HER catalysis has been focused on several important parameters such as the intrinsic nature of the reaction [8,9,18,19], electrode composition [20–24], surface morphology [8,9,18,24–29], structural, chemical, and electronic properties [20–23,30], and physical, chemical, and electrochemical activation treatments [8,9,18,31–33].

The present work discusses results on the use of conducting polymers, polypyrrole, and polyaniline, as a support/matrix/template for the construction of nickel/conducting polymer hydrogen evolution catalyst layers. Nickel has been chosen as a catalytic material due to its high intrinsic activity in the HER and its low cost compared to noble metals currently used in the construction of PEM hydrogen generators. The two conducting polymers have been chosen due to their (i) insulating properties in the cathodic region relevant for hydrogen production, thus avoiding their catalytic interference with the HER charge transfer process and Ni catalysts, (ii) favorable pattering morphology, (iii) stability in the PEM environment of a hydrogen generator (low pH), (iv) high solubility in aqueous solutions, (v) well-developed and simple electrochemical polymerization methodology, and (vi) suitability for a potential commercial use. Although electrocatalysis on conducting polymer-based layers incorporating metal particles (mostly Pt or other noble metals) has been reported in literature, the majority of the work is related to oxidation reactions [34–39], while reduction reactions have been much less studied, and are mainly concentrated in the area of oxygen reduction [40–43]. The application of conducting polymers doped with metallic inclusions in gas sensing applications has also been reported [44]. However, to the best of our knowledge, only few publications discussing the use of conducting polymers in hydrogen reduction (production) have been reported [45–48]. In Ref. [47], no metal particles were incorporated into the polypyrrole film but the HER actually took place at the substrate (iron) surface. On the other side, in Ref. [48], electroless nickel was used as a catalyst incorporated into a polypyrrole film but the substrate chosen was platinum. However, the actual catalytic effect of incorporated nickel particles in the HER was difficult to distinguish from the catalytic effect of the Pt substrate due to the porosity of the polymer layer, as studied in Ref. [49].

This paper represents an attempt to contribute to the development of active, efficient, stable, and cheap nickel electrocatalysts for hydrogen production by water electrolysis in the PEM hydrogen generator. It will be demonstrated that the two conducting polymers (CP) represent good three-dimensional matrices that can be conveniently employed to tailor morphology of electrocatalytic Ni layers used in hydrogen production. Four different morphologies can be obtained, each yielding a different electrocatalytic activity in the HER, when compared to a Ni layer deposited on a flat two-dimensional conducting substrate. It will also be shown that the structure of the Ni–CP layer and Ni/CP–electrolyte interface strongly depends on the morphology of the prepared Ni/CP layers and the type of polymer used.

2. Experimental

The electrocatalytic activity of nickel/conducting polymer (Ni/CP) layers in the hydrogen evolution reaction was studied in 0.5 M H_2SO_4 solution at 295 K. Chemicals used in research were purchased from Sigma–Aldrich Company and Fisher Scientifics, and were used without further purification. All solutions were prepared using nanopure water of resistivity 18 MΩ cm. All measurements were made in an oxygen-free solution, which was achieved by continuous purging of the cell electrolyte with argon gas (99.998% pure).

A standard three-electrode, two compartment cell was used in all experiments. The counter electrode was a large-area platinum electrode of high purity (99.99%, Alfa Aesar), which was degreased by refluxing in acetone, sealed in soft glass, electrochemically cleaned by potential cycling in 0.5 M sulfuric acid, and stored in 98% sulfuric acid. During measurements, the counter electrode was separated from the main cell compartment by a glass frit. The reference electrode was a commercially available mercury/mercurous sulfate electrode (MSE).

Table 1
Experimental conditions used in formation of Ni/CP layers on a GC substrate

Bath	Composition		Ni/CP-layer formation conditions
Nickel	$NiSO_4 \cdot H_2O$	26.2 g L^{-1}	Deposition potential: −1.45 V_{SCE}
	H_3BO_3	6.2 g L^{1}	
	H_2SO_4	1.0 mM	
Pyrrole	Pyrrole	0.05 M	Deposition potential: 0.8 V_{SCE}
	H_2SO_4	0.5 M	
Polyaniline	Aniline	0.05 M	Deposition potential: 0.82 V_{SCE}
	H_2SO_4	0.5 M	
Co-deposition	Ni + pyrrole bath		Potential range: +0.8 and −1.45 V_{SCE} Delay at +0.8: 3 s Delay at −1.45: 5 s Scan rate: 100 mV s^{-1}

The working electrode was a Ni/CP layer electrodeposited on a glassy carbon (GC) substrate of surface area 0.17 cm^2. GC was chosen as a substrate material since it has very large overpotential for hydrogen evolution, thus offering a wide potential region for the investigation of the HER, without the substrate interference. The GC electrode (substrate) was made of a rectangular piece of GC sealed in an epoxy, thus giving a two-dimensional surface area available for the electrodeposition of an electrocatalytic layer. Before electrodeposition of a Ni/CP layer, the GC substrate was carefully prepared by mechanical wet-polishing using #600 and #1500 grit sand paper, followed by thorough rinsing with distilled water and cleaning in an ultrasonic bath for 6–7 min in order to remove polishing residues. Subsequently, the substrate was degreased with ethanol, rinsed with nanopure water, and further electrochemically cleaned (activated) in 0.5 M H_2SO_4 by potentiodynamic cycling between the hydrogen and oxygen evolution potential. The formation of active Ni/CP layers was done (i) by potentiostatic electrodeposition of Ni on a polypyrrole or polyaniline layer pre-deposited on a GC substrate and (ii) by cyclic co-electrodeposition of Ni and polypyrrole on a GC substrate. The experimental conditions and baths composition are presented in Table 1. After the formation of each electrode layer, the electrode surface was carefully rinsed with a large amount of nanopure water in order to remove any residues of bath chemicals and unattached catalyst particles. Then, the electrode was placed in the electrochemical cell, and in order to reduce any nickel oxides spontaneously formed on the catalyst surface, i.e. to activate the electrocatalyst, the electrode was polarized at −0.50 V (versus SHE) for 5 min, followed by stabilization at OCP until a steady-state OCP value was obtained (usually less then 5 min). Then, the linear polarization measurement was made, starting from the OCP to potential OCP-500 mV, at a scan rate of 0.5 mV s^{-1}. The dc polarization measurement was followed by a set of ac EIS measurements at selected potentials in the range between OCP and OCP-500 mV. An Autolab PGSTAT 30 potentiostat/galvanostat/FRA was used in all the electrochemical measurements, while the scanning electron microscopy (SEM) analysis was done using a Hitachi 4700 field emission SEM. All the dc polarization curves were corrected for the *IR*-drop.

3. Results and discussion

3.1. Morphology of polypyrrole and polyaniline

As mentioned in the Introduction, conducting polymers, PPY and PANI were used as three-dimensional (3D) 'pattering templates' (matrices) for controlled morphological structuring of Ni catalyst layers. The hypothesis of the authors was that this procedure would enable formation of a layer that would offer a 3D hydrogen evolution reaction zone, and thus an increase in the surface area and number of activation sites for the reaction. Morphology of conducting polymer layers (matrices) deposited on a glassy carbon substrate was first characterized using a scanning electron microscopy technique. The SEM images in Fig. 1a and b show a significant difference in the morphology of the two polymers. The PPY matrix electrodeposited on the GC surface (Fig. 1a) offers a compact and homogeneous micro/nano-porous surface. As it will be shown later, these micro/nano-pores provide electrolyte-conducting pathways to the GC substrate for electrochemical deposition and growth of nickel catalyst 'islands'. On the other hand, the PANI matrix presented in Fig. 1b shows a significantly different morphology. The matrix has a highly fibrilar, branched, and porous structure, with an average thickness of fibers of ca. 100 nm. Taking into account the difference in the morphology of the two polymer matrices observed in Fig. 1a and b, one could conclude that the deposition of a Ni catalyst layer inside the 3D CP structure should also result in a significant difference in the morphology of the resulting composite Ni/CP layers.

3.2. Linear dc polarization measurements

3.2.1. Ni/PPY electrocatalytic layers

In order to investigate the influence of the morphology of the CPs on a relative electrocatalytic activity of formed Ni/CP catalytic layers, linear Tafel polarization measurements were made, and the corresponding electrochemical parameters (Tafel slope, exchange current density, transfer coefficient) were derived from the recorded curves. Fig. 2 shows the representative linear polarization curves recorded on Ni/PPY catalysts. All the curves presented show a classical Tafelian behavior in the lower over-

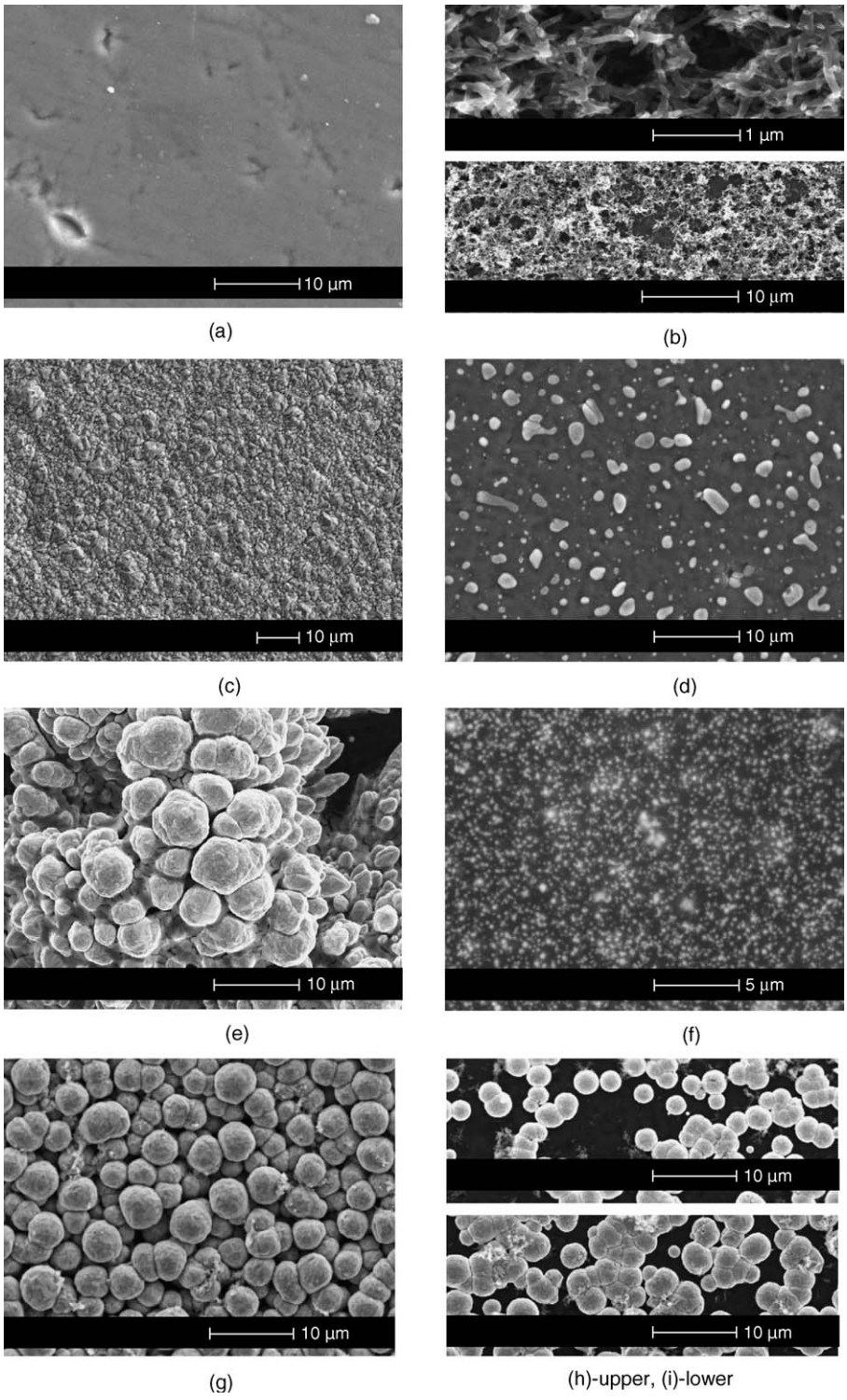

Fig. 1. SEM images showing the surface morphology of (a) polypyrrole (PPY) and (b) polyaniline (PANI) electrodeposited on a GC substrate. The other images show electrodes made by (c) electrodeposition of Ni on a Cu substrate, (d) electrodeposition of Ni for 20 min on a PPY layer pre-deposited for 2.5 min (GC substrate), (e) electrodeposition of Ni for 1 h:40 min on a PPY layer pre-deposited for 2.5 min (GC substrate), (f) simultaneous co-electrodeposition of Ni and PPY (GC substrate), (g) electrodeposition of Ni for 20 min on a PANI layer pre-deposited for 2.5 min (GC substrate), and electrodeposition of Ni for (h) 2 min and (i) 5 min on a PANI layer pre-deposited for 2.5 min (GC substrate).

potential region, i.e. at overpotentials positive of ca. −0.4 V. This clearly demonstrates that the HER on all the Ni/PPY catalysts is a purely kinetically controlled reaction. An average value of the Tafel slope obtained in this region is $135 \pm 4\,\text{mV decade}^{-1}$. According to the general models of the HER mechanisms in an acidic medium [50,51,52], this value of Tafel slope indicates that the Volmer reaction step, i.e. adsorption of hydrogen on nickel to form Ni–H_{ads}, is a rate determining step. It could also be noticed

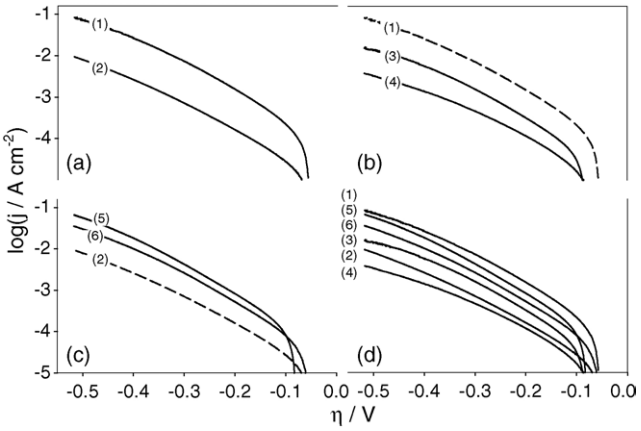

Fig. 2. Linear polarization curves recorded on Ni/PPY electrodes: (1) Ni/PPY-1:40/2.5, (2) Ni/PPY-20/2.5, (3) Ni/PPY-1:40/5, (4) Ni/PPY-20/5, (5) Ni/PPY-Co-40, and (6) Ni/PPY-Co-20. Scan rate = 0.5 mV s^{-1}. The curves were corrected for the *IR*-drop.

that the measured Tafel slope value slightly deviates from the theoretical value of 116 mV $decade^{-1}$. This phenomenon has already been reported in literature [17,25,26,53] and has been explained by the presence of a thin oxide film on the catalyst's surface [17,24].

The purpose of doing the experiments presented in Fig. 2 was to investigate the influence of Ni and/or PPY deposition time and method on the resulting HER activity of the catalysts. Fig. 2a demonstrates the effect of Ni electrodeposition time on the resulting catalyst's response in the HER. Nickel was electrodeposited on an already pre-deposited PPY layer (PPY deposition time was 2.5 min). It is evident that the catalyst produced by electrodeposition of Ni at a longer time, 1 h:40 min (curve 1, Ni/PPY-1:40/2.5), shows a significantly higher activity in the HER than the catalyst produced by electrodeposition of Ni at a shorter time, 20 min (curve 2, Ni/PPY-20/2.5). The difference in the activity is approximately of one order of magnitude. Since the same electrocatalytic material, Ni, was used in both cases, the observed difference should thus be related mainly to the difference in the surface area available for the HER, i.e. the difference in the number of electroactive sites available for the reaction, rather than to the difference in the intrinsic activity of the two catalysts (electronic effect). In order to investigate this more closely, the morphology of both catalysts was examined using the SEM technique. Fig. 1d shows the morphology of the Ni/PPY-20/2.5 catalyst, while a morphology of the catalyst produced by electrodeposition of Ni at a longer time, Ni/PPY-1:40/2.5, is presented in Fig. 1e. As expected, the difference in the electrocatalytic activity in the HER shown in Fig. 2a is quite in accordance with the difference in the morphology of the two surfaces. Fig. 1d shows that at shorter Ni electrodeposition times the distribution of Ni catalyst islands is uniform. However, the island size distribution is rather wide, ranging from ca. 100 nm to 3 μm, which is most likely controlled (pre-determined) by the diameter of pores inside the PPY layer formed on the electrode surface before Ni electrodeposition. The mechanism of the formation of Ni islands and the resulting surface morphology could be explained in the following manner. Since PPY is

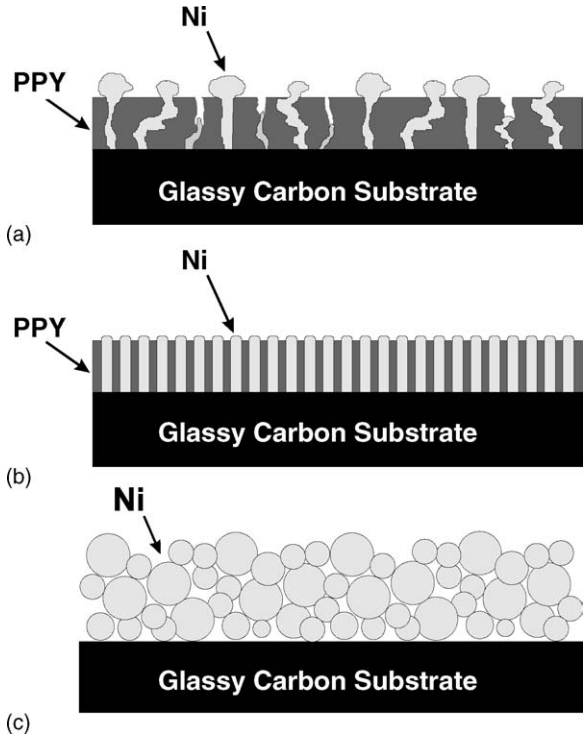

Fig. 3. Schematic representation of Ni/CP catalyst layers produced by (a) deposition of Ni on a pre-deposited PPY layer, (b) co-deposition of Ni and PPY, and (c) deposition of Ni on a pre-deposited PANI layer.

not electrically conductive in the region of Ni electrodeposition, nucleation of Ni islands cannot occur on top of, or inside the PPY matrix. Therefore, Ni islands start forming by nucleation (electrocrystallization) at the GC/electrolyte interface, on the part of electrically conductive GC surface that is directly exposed to the bulk electrolyte through pores of the pre-deposited PPY layer. The formed nuclei continue to grow in an outward direction through the PPY pores towards the bulk electrolyte (Fig. 3a) [54,55]. Since the distribution of pore length, diameter and configuration in the pre-formed PPY layer is not uniform, it could be assumed that some Ni islands do not reach the outer surface of the polymer at the shorter electrodeposition time (20 min, Figs. 1d and 3a), and could remain 'arrested' at various depths inside the polymer matrix. On the other side, some of the islands continue growing above the PPY layer surface in a semi-lateral direction, forming mushroom-type islands that are quite visible in Fig. 1d. The image also shows small-diameter Ni islands that reached only the PPY surface and did not start spreading above it in a semi-lateral direction. Similar morphology was observed on Cu/PPY composite layers [56]. From this analysis, it is obvious that the density, distribution, diameter, and configuration of Ni islands on the electrode surface at shorter Ni deposition times is mostly pre-determined by the same three parameters related to the pre-deposited PPY layer. This, in turn, opens a wide range of possibilities for producing various morphologies of metallic electrocatalyst layers by simple tailoring (controlling) morphological properties (templates) of PPY layers.

When Ni is electrodeposited on an electrode surface free of PPY, the resulting metal layer is continuous and of a 2D-like

morphology (Fig. 1c). Thus, one would expect that a long-term deposition of Ni on a pre-deposited PPY layer would also give a continuous semi-2D compact Ni layer similar to the one in Fig. 1c, which would be formed by the growth and merger of neighboring islands shown in Fig. 1d. However, Fig. 1e demonstrates that at longer Ni deposition times metal islands continue growing outside the PPY layer in a 3D manner, forming very interesting spherical (globular) and cauliflower-like patterns. The size of globules ranges from ca. 1 to 10 μm. The resulting morphology (Fig. 1e) yields a considerably rougher surface than the Ni layer deposited at shorter times (Fig. 1d) and in the absence of PPY (Fig. 1c). As a result, an increase in activity in the HER is observed (Fig. 2a). Hence, it appears that the presence of PPY on the electrode surface significantly influences the mechanism of Ni growth outside the PPY matrix. This might be due to the hydrophobic character of the PPY layer, which repels hydrated nickel ions and thus inhibits the spreading (growth) of Ni islands along the PPY/electrolyte interface in a 2D manner, facilitating the 3D growth into the bulk electrolyte.

The above discussion leads to a conclusion that a thicker PPY layer deposited at longer times would be less porous, due to the narrowing and blockage (termination) of pores caused by lateral growth of the polymer. Thus, an increase in the pore length (by thickening of the PPY layer), and decrease in the pore diameter and density (by the lateral growth/expansion of the PPY layer), would then result in an increased resistance to mass transport of nickel ions to the GC surface. Consequently, a decrease in the amount of nickel deposited on the electrode surface, and thus the total surface area of the catalyst available for the HER, could be expected. This assumption is clearly confirmed in Fig. 2b, which demonstrates that an increase in the PPY layer thickness (by doubling its formation time from 2.5 to 5 min) results in a decrease in catalytic activity of the electrode down to ca. 22% of its initial value (compare curves 3 and 1 in Fig. 2b). Also, similarly to the situation in Fig. 2a, the electrode produced at longer Ni deposition times (Fig. 2b, curve 3, Ni/PPY-1:40/5) yields a higher activity when compared to the electrode produced at shorter Ni deposition times (Fig. 2b, curve 4, Ni/PPY-20/5). The results in Fig. 2a and b suggest that a thinner PPY layer offers a higher porosity, which allows for a higher density of Ni islands to be formed on the electrode surface. However, this positive effect is partially counterbalanced by a negative effect related to a decrease in the surface area of the Ni layer due to a decrease in the PPY pore length, and thus also the Ni island length (height). Our measurements have shown that, under the experimental conditions applied here, an optimum PPY thickness is obtained at a PPY deposition time of 2.5 min.

In order to optimize the structure of the catalyst layer and achieve a higher degree of control over the composite layer morphology, formation of both the PPY and nickel layer should be done in parallel. The idea of the authors was to first deposit a very thin and highly porous layer of PPY on the GC surface (a few angstroms thick). This layer would then serve as a surface template grid for the subsequent deposition of Ni in the pores of this PPY layer until reaching the same thickness. Then, a second PPY layer would be deposited on top of the initially formed PPY layer, following the initial morphological pattern. Again, this would be followed by the formation of the second Ni layer. This co-deposition procedure could be repeated for a desired number of cycles until a specified layer thickness is achieved, which is schematically presented in Fig. 3b. In this way, a long-nano-island structure of the Ni layer, offering a high Ni island density, narrower island diameter distribution and a more controlled layer growth and morphology, could be achieved. An experimental technique applied for this purpose was cyclic voltammetry. An initial potential was set in the anodic potential region of pyrrole polymerization, 0.8 V versus SCE, while a cathodic limit was in the potential region of Ni electrodeposition, −1.45 V versus SCE (see Table 1). Fig. 1f shows a morphology of a catalyst produced using this co-deposition procedure. In comparison to Ni/PPY-20/2.5 layer produced by electrodeposition of Ni on a pre-deposited PPY layer (Fig. 1d), the co-deposition procedure offers a morphology characterized by a considerably higher density of Ni islands formed on the surface. In addition, the diameter of Ni islands is smaller (between 100 and 300 nm) and their distribution more uniform. Similar surface morphology was reported for composite layers produced by incorporation of Pt particles into a polythiophene [41] and polypyrrole [57] layer, and gold particles into a polypyrrole layer [55]. However, in these works metal particles were produced either by electroreduction of anions of their salts ($PtCl_4^{2-}$) pre-incorporated in the polymer layer during its polymerization, or by subsequent electrodeposition of metal (Au) on a pre-deposited PPY layer.

Considering the morphology presented in Fig. 1f, one could expect to see an increase in catalytic activity with respect to the surface in Fig. 1d. This is, indeed, demonstrated in Fig. 2c, from which it is clearly visible that the surfaces produced using the co-deposition method (solid curves 5 and 6) show a higher electrocatalytic activity in the HER than the surface produced by electrodeposition of Ni on a pre-deposited PPY layer (dashed curve 2). By applying a higher number of co-deposition cycles, a further increase in the electrocatalytic activity is achieved (curve 5 = 40 cycles and curve 6 = 20 cycles). However, our measurements have demonstrated that the relationship between the number of co-deposition cycles and the corresponding electrocatalytic activity of the catalyst is not linear, but rather logarithmic. At high overpotentials, accumulation of molecular hydrogen produced deep inside the catalyst layer occurs. This results in a partial blockage of that portion of the Ni surface for the HER. With an increase in overpotential, the amount of produced hydrogen also increases, and thus the area of the catalyst surface blocked by hydrogen. This is clearly seen on all the curves in Fig. 2, where a deviation from linearity is apparent at overpotentials negative of ca. −0.4 V, especially on the two catalysts produced by deposition of Ni in a thicker PPY film (Fig. 2d, curves 3 and 4). The solution to the problem would be to remove (dissolve) the PPY film once the Ni layer is formed. Further, by combining the co-deposition procedure and subsequent removal of the PPY layer, an open-nano-island structure of the Ni layer could be achieved. This would offer a large increase in the surface area available for the HER and also prevent accumulation of produced hydrogen (blockage of the catalyst surface). This is

a topic of current research in our laboratory and will be reported shortly.

In order to relatively compare all the Ni/PPY catalysts presented so far, the corresponding linear polarization curves are plotted on the same graph (Fig. 2d). A close inspection of the plot reveals that the best electrocatalytic performance is offered by the Ni/PPY-1:40/2.5 electrode produced by electrodeposition of Ni for a longer time on a thin pre-deposited PPY layer. An opposite result is obtained when a long PPY deposition time (5 min) and short Ni deposition time (20 min) is used (Ni/PPY-20/5 electrode). The electrodes made using a co-deposition method offer an intermediate performance. However, this needs some clarification. When a co-deposition method is used, an actual time of Ni deposition is much shorter than when Ni is deposited on a preformed PPY layer. For example, when 40 cycles are used in the co-deposition procedure (Table 1), the actual Ni deposition time is 1 min 20 s, which results in a much lower loading of Ni, when compared to Ni/PPY-20/2.5. Still, Ni/PPY-Co-40 yields much better electrocatalytic activity than Ni/PPY-20/2.5. This is due to a favorable structure of the catalyst (Fig. 1f), which offers a considerably larger surface area for the HER then Ni/PPY-20/2.5 (Fig. 1d). Our recent measurements have shown that by increasing a number of co-deposition cycles above 40, a substantial increase in the electrode activity above the level shown by Ni/PPY-Co-40 is obtained.

3.2.2. Ni/PANI electrocatalytic layers

Figs. 1a and b shows that the morphology of a PANI layer is considerably different than the morphology of a PPY layer. Hence, one could expect to see a difference in the morphology of the corresponding Ni/CP layers. Fig. 1g shows an image of a catalyst layer produced by electrodeposition of Ni on a pre-deposited PANI layer. Indeed, the difference in the morphology between the Ni/PANI (Fig. 1g) and Ni/PPY (Fig. 1d–f) layers is substantial. While all the Ni/PPY layers are compact and show the presence of both the polymer and metallic phase, the Ni/PANI electrode is covered by only a three-dimensional layer of spherical Ni particles of an average diameter 3 μm. The image shows the presence of only traces of PANI residues attached to Ni particles, and a complete absence of a continuous PANI phase can be observed. Fig. 1h and i shows morphology of Ni/PANI catalysts produced at short Ni deposition times, 2 and 5 min, respectively. It is evident that the nucleation of a Ni phase starts on the electrically conductive GC surface, followed by its 3D growth to form spherical particles. By comparing the three SEM PANI images (Fig. 1g–i), it seems that with an increase in deposition time a growth rate of Ni spheres decreases after several minutes, and almost drops to zero when spheres reach an average diameter of 3 μm. However, at the same time, the nucleation and growth of new spherical particles occurs in parallel, resulting in an increase in the number of particles formed on the surface (density). Hence, the surface coverage increases going from Fig. 1h, over i to g. At longer deposition times the Ni layer grows to a thickness of at least three mono-spherical layers (Fig. 1g), offering a highly porous structure that is schematically presented in Fig. 3b. Considering fibrous morphology of the PANI layer presented in Fig. 1b, it is quite surprising to see a

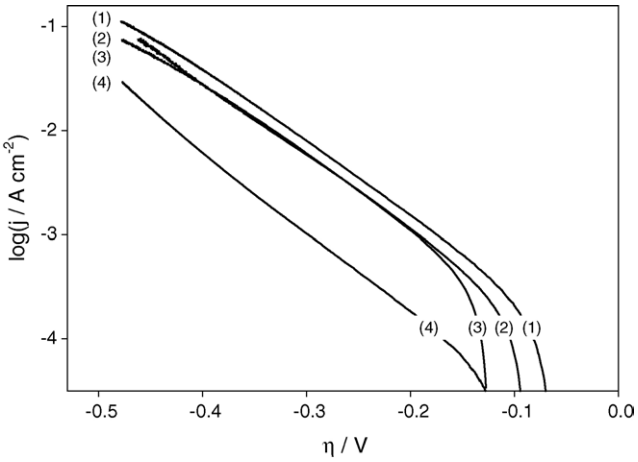

Fig. 4. Linear polarization curves recorded on Ni/PANI electrodes: (1) Ni/PANI-20/5, (2) Ni/PANI-1:40/2.5, (3) Ni/PANI-1:40/5, (4) Ni/PANI-20/2.5. Scan rate = 0.5 mV s^{-1}. The curves were corrected for the *IR*-drop.

globular-like structure of the produced Ni layer. At the moment it is not clear what could be a fundamental reason for such a large difference in the observed structure/morphology transformation, but the influence of hydrophobic, structural (fibrous) or surface charge distribution properties of the PANI layer could be one of the possible effects.

Fig. 4 shows a set of polarization curves recorded on various Ni/PANI catalysts. An influence of Ni and/or PANI deposition time on the resulting electrocatalytic activity was investigated. Curve 1 represents a response of the best catalyst, produced by electrodeposition of Ni for 20 min on a PANI layer pre-deposited for 5 min (Ni/PANI-20/5). A significantly lower electrocatalytic activity was obtained if a PANI deposition time was decreased to 2.5 min (curve 4, Ni/PANI-20/2.5). This is quite different to the results obtained on Ni/PPY catalysts (Fig. 2b), but is also reasonable to expect considering a large difference in the structure (and porosity) of the two CP layers and their role on the mechanism of Ni phase nucleation and growth. When a Ni layer is formed on the pre-deposited PPY layer, its growth occurs only through pores of the PPY layer, as previously discussed. The presence of both the polymer and metallic Ni phase on the surface of the Ni/PPY catalysts (Fig. 1d–f) indicates that the growth of the Ni phase does not significantly influence the stability of the PPY phase. On the other hand, it appears that the growth of a Ni phase on the pre-deposited PANI layer results in a disappearance of the polymer phase. Since the PANI layer acts also as a 'surfactant', and not only as a pattering template (such as PPY), it seems that in order to produce more Ni spherical particles (i.e. a thicker Ni layer), a thicker PANI film is needed. This is indeed observed in Fig. 4 (curves 1 and 4). On the other hand, if the Ni layer is deposited at a long time (1 h:40 min), the thickness of the pre-deposited PANI layer appears not to have a large influence on the resulting electrocatalytic activity and the two polarization curves in Fig. 4 (curves 2 and 3) are overlapped. Also, a decrease in the activity, when compared to Ni/PANI-20/5 (curve 1), is observed. The reason for this might be either due to a partial decrease in porosity of the Ni layer, or due to the agglomeration of spherical Ni particles. Neverthe-

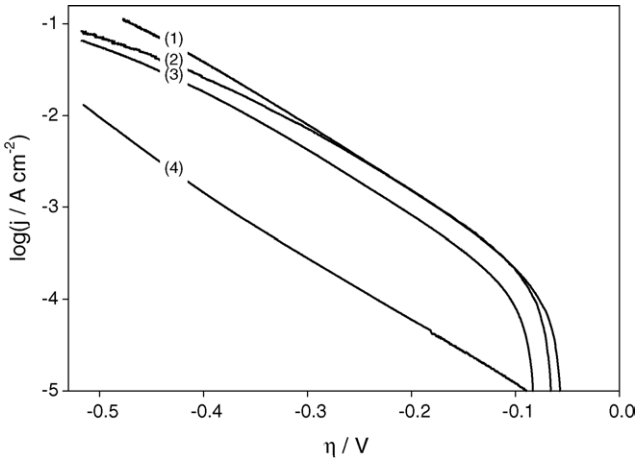

Fig. 5. Linear polarization curves recorded on (1) Ni/PANI-20/5, (2) Ni/PPY-1:40/2.5, and (3) Ni/PPY-Co-40. A curve recorded on a Ni catalysts deposited on a Cu substrate (Ni/Cu) is also presented for comparison (4). Scan rate = 0.5 mV s^{-1}. The curves were corrected for the *IR*-drop.

less, even at long Ni deposition times the porosity of the layer is sufficiently large to allow hydrogen produced at high overpotentials to diffuse into the bulk solution, thus avoiding the blockage of the catalyst's surface observed with all the Ni/PPY catalysts. Consequently, no deviation from the linearity of the polarization curves in Fig. 4 is noticed at high cathodic overpotentials.

3.2.3. *Relative comparison of Ni/PPY and Ni/PANI electrocatalytic layers*

In order to compare a relative electrocatalytic activity of the Ni/CP layers that gave the highest electrocatalytic activity within the group, the Tafel curves recorded on the best group catalysts studied have been plotted on the same graph (Fig. 5), together with a Tafel curve of a semi-2D Ni layer deposited on a flat Cu substrate (control curve). The plot offers a clear picture on the performance of all the 'best' HER composite Ni/CP catalysts. The relevant kinetic data obtained by analysis of the curves are presented in Table 2.

From Fig. 5 and Table 2, it can be observed that all the Tafel curves yield a similar Tafel slope value, and that there is no evidence on the change of the reaction mechanism with the increase in overpotential. Comparing the calculated values of transfer coefficients, α, of the Ni/CP catalysts to the value of the control catalyst (Ni/Cu), Table 2, it seems that all the Ni/CP catalysts offer slightly higher electrocatalytic activity in terms of the invested energy used for the HER. This could be due to a favorable electronic influence of the CP matrix on the intrinsic activity of Ni (catalyst/support interaction). On the other hand, the exchange current density values presented in the table demonstrate a superior electrocatalytic activity of the Ni/CP catalysts at the equilibrium HER potential (zero overpotential), relative to the Ni/Cu catalyst. Ni/PANI-20/5 offers the highest activity, almost 20 times higher than Ni/Cu catalyst. However, although the exchange current density is very frequently used to characterize an electrocatalytic activity of a catalyst, it is more appropriate to evaluate a catalytic activity at some fixed current or overpotential that is relevant to the actual operation of the hydrogen generator. This is very important in cases when different catalysts yield different Tafel slope values [27]. Hence, in order to compare the electrocatalytic activity of the catalysts in Fig. 5 at conditions relevant for the operation of a hydrogen generator, one can fix current density (i.e. hydrogen production rate) and compare the resulting overpotentials required to reach the given current density. This would give an indication on the amount of energy (overpotential) that has to be invested to produce a specified amount of hydrogen (since the current is, through the Faraday law, directly related to the amount of produced hydrogen). Overpotential values for each catalyst measured at a fixed current density of 1 mA cm^{-2} are presented in Table 2. It is obvious that Ni/Cu requires the largest energy input (overpotential) for the given hydrogen production rate, −379 mV, while Ni/PANI-20/5 requires the lowest energy input, overpotential −175 mV. This represents an energy saving of ca. 53%.

Another common way of comparing the electrocatalytic activity of HER electrocatalysts is to fix overpotential (energy input) and then to compare the resulting current densities, i.e. the amount of hydrogen that would be produced by each catalyst. The results for overpotential of −150 mV (which is in the range expected for a hydrogen generator operation) are presented in Table 2. Again, similarly to the behavior obtained at a fixed current density, Ni/PANI-20/5 yields the best electrocatalytic activity. The amount of hydrogen that could be produced using Ni/PANI-20/5 is ca. 24 times larger than if Ni/Cu were used. Comparing the data in Table 2 and lower overpotential region in Fig. 5, it is evident that the performance of Ni/PANI-20/5 and Ni/PPY-1:40/2.5 is practically the same. However, at high overpotentials, Ni/PANI-20/5 offers higher electrocatalytic activity. This is due to a favorable porous 3D structure of the catalyst layer, which ensures that no accumulation of produced hydrogen inside the layer occurs, contrary to Ni/PPY-1:40/2.5 catalyst. In conclusion, the electrocatalytic activity trend evaluated at con-

Table 2
HER kinetic parameters (b, j_o and α) obtained by analysis of the curves presented in Fig. 5

Catalyst	b (mV decade^{-1})	j_o (μA cm^{-2})	α	η (mV) at 1 mA cm^{-2}	j (mA cm^{-2}) at −150 mV
Ni/Cu (control)	147	−2.6	0.39	−379	−0.027
Ni/PANI-20/5	133	−47.3	0.44	−175	−0.647
Ni/PPY-1:40/2.5	133	−45.9	0.44	−176	−0.629
Ni/PPY-Co-40	134	−25.7	0.43	−222	−0.334

The table also shows the data used to compare the electrocatalytic activity of the investigated Ni/CP coatings in terms of (a) the overpotential needed for a fixed hydrogen production rate determined by a current density of 1 mA cm^{-2} and (b) the resulted production rate at a fixed energy input (fixed overpotential of −150 mV). The results for a control catalyst (Ni/Cu) are also presented for comparison.

ditions relevant for the operation of a hydrogen generator is the same as the trend observed at equilibrium conditions (using the exchange current density), and shows that the electrocatalytic activity of the investigated catalysts decreases in the direction of Ni/PANI-20/5 ≥ Ni/PPY-1:40/2.5 > Ni/PPY-Co-40 > Ni/Cu.

The information obtained from the Tafel polarization data shows that all the Ni/CP catalysts are more active for the HER than the control catalyst, Ni/Cu, which is mainly due to an increase in the number of HER active sites, i.e. surface area increase. Only a small contribution of the electronic effect (catalyst/support interaction) is observed.

3.3. Electrochemical impedance spectroscopy (EIS)

Although the SEM and dc Tafel polarization techniques gave information on the morphology and overall electrocatalytic activity of the Ni/CP layers studied, these techniques cannot provide information on the structure of the electrode/electrolyte interface in terms of the surface charge and electroactive centers distribution, and hydrogen adsorption. Therefore, electrochemical impedance spectroscopy was employed to further investigate the electrode/electrolyte interface and the corresponding processes that occur at the electrode surface. To ensure a complete characterization of the electrode/electrolyte interface and corresponding processes, EIS measurements were made over six frequency decades, from 50 kHz to 50 mHz, at selected overpotentials in the whole overpotential range covered with linear polarization plots (ca. from the OCP to OCP-500 mV). As it will be shown, the EIS technique revealed new information on the structure of the electrode/electrolyte interface and on the spatial distribution of electroactive centers in three-dimensional Ni/CP layers.

3.3.1. Ni/PPY electrocatalytic layers

Fig. 6 shows an example of EIS spectra recorded on Ni/PPY-20/5 at several selected overpotentials. The data are represented in a form of both Nyquist (Fig. 6a) and Bode (Fig. 6b) plot. All the spectra on the Nyquist plot display a semicircular trend, which is consistent with EIS data obtained on other HER electrocatalysts [17,52]. With an increase in overpotential, the diameter of the semicircle decreases, which, in the first approximation, reflects a decrease in the HER resistance, and thus, through the Ohm law, an increase in HER current [17]. Since the resistance is inversely related to current (i.e. hydrogen production rate), a consistent relationship should exist between dc Tafel plots and ac resistance plots which will be demonstrated later (Fig. 9). The data in Fig. 6a also show that the semicircles are not symmetrical, but a small deviation (distortion) at low frequencies (higher real impedance, Z′, values) is noticeable, especially at a low overpotential. This indicates that the recorded EIS behavior is rather complex and represents a response of a process characterized by at least two time constants [17,27,58,59]. Indeed, the presentation of the data in a form of Bode impedance plot (Fig. 6b) clearly reveals the presence of two time constants, namely a high frequency (HF) time constant above ca. 200 Hz, τ_1, and a low frequency (LF) time constant below ca. 200 Hz, τ_2. Therefore, in order to obtain a physical picture of the electrode/electrolyte

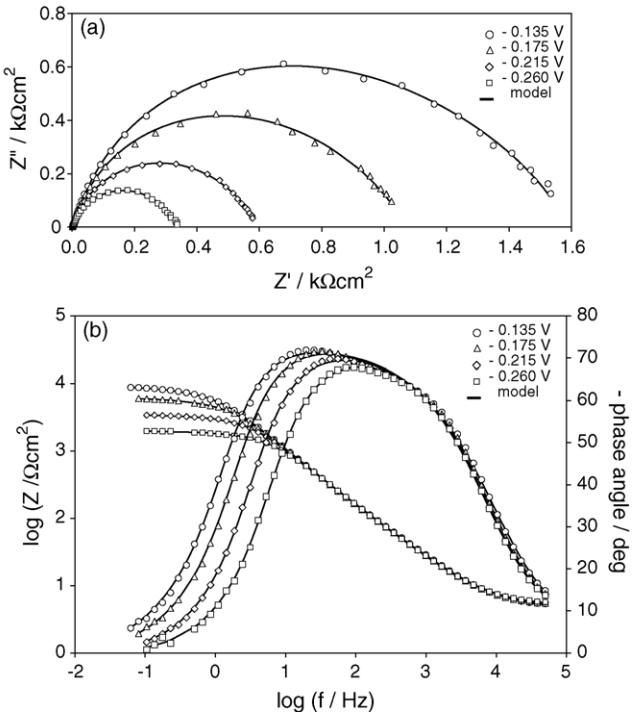

Fig. 6. (a) Nyquist and (b) Bode plots showing an EIS response of the Ni/PPY-20/5 electrode at various overpotentials. Symbols are experimental and solid lines are modeled data.

interface and the processes occurring at the electrode (catalyst) surface, experimental EIS data were modeled using non-linear least-squares fit analysis (NLLS) software [60] and an electrical equivalent circuit (EEC) that describes a response of a two-time constant process, inset to Fig. 7. An excellent agreement between the experimental data (symbols) and modeled data (lines) was obtained (Fig. 6), and the calculated EEC data are presented

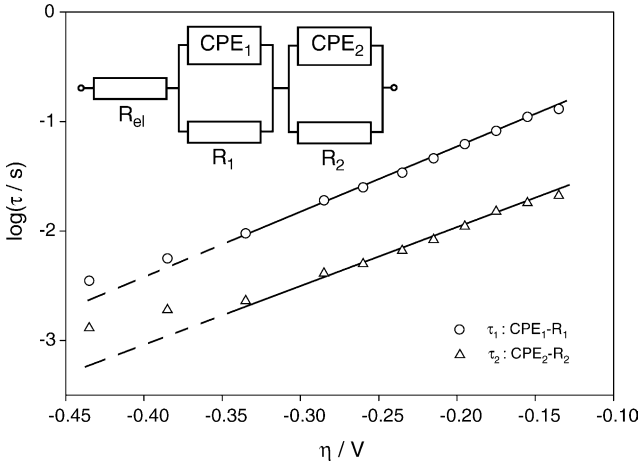

Fig. 7. Semi-logarithmic dependence of time constants on applied overpotential calculated by modeling EIS data recorded on Ni/PPY-20/5. The data were modeled using the electrical equivalent circuit (EEC) presented as an inset to the figure. $R_{el}(CPE_1 - R_1)(CPE_2 - R_2)$ circuit was used to model the data obtained on Ni/PPY electrodes, while $R_{el}(CPE_1 - R_1)$ circuit was used to model the data recorded on Ni/PANI electrodes. R_{el} represents the resistance of the electrolyte between the working and reference electrode. The physical meaning of the remaining EEC elements is given in the text.

Table 3
EEC parameters obtained by fitting EIS experimental spectra recorded at various overpotentials on the Ni/PPY-20/5 electrode

η (V)	R_{el} (Ω)	$CPE_1 \times 10^4$ ($F\,s^{n-1}\,cm^{-2}$)	n_1	R_1 ($\Omega\,cm^2$)	$CPE_2 \times 10^4$ ($F\,s^{n-1}\,cm^{-2}$)	n_2	R_2 ($\Omega\,cm^2$)	$C_{dl,1}$ ($\mu F\,cm^{-2}$)	$C_{dl,2}$ ($\mu F\,cm^{-2}$)	τ_1 (s)	τ_2 (s)
−0.115	4.4	1.8	1.0	790	4.2	0.73	860	180	20	1.4E−01	1.7E−02
−0.135	4.4	1.7	1.0	717	5.0	0.72	874	170	24	1.3E−01	2.1E−02
−0.155	4.6	1.7	1.0	622	4.9	0.73	716	170	25	1.1E−01	1.8E−02
−0.175	4.6	1.6	1.0	511	5.3	0.72	556	160	26	8.2E−02	1.5E−02
−0.195	4.8	1.7	1.0	374	4.8	0.73	420	170	27	6.2E−02	1.1E−02
−0.215	4.9	1.6	1.0	293	5.0	0.73	299	160	28	4.6E−02	8.3E−03
−0.235	4.9	1.6	1.0	215	4.8	0.73	238	160	28	3.4E−02	6.6E−03
−0.260	5.0	1.5	1.0	162	4.9	0.73	175	150	29	2.5E−02	5.0E−03
−0.285	5.1	1.6	1.0	115	4.1	0.75	142	160	29	1.9E−02	4.1E−03
−0.335	5.1	1.5	0.97	81	5.2	0.74	74	120	32	9.5E−03	2.3E−03
−0.385	5.0	1.7	1.0	32	3.5	0.76	69	170	28	5.6E−03	1.9E−03
−0.435	5.1	1.8	1.0	19	3.0	0.77	47	180	27	3.5E−03	1.3E−03

in Table 3. The fitting procedure showed that a better agreement between theoretical and experimental data was obtained when pure capacitance was replaced by a frequency-dependent constant-phase element, CPE ($\Omega^{-1}\,s^n\,cm^{-2}$ or $F\,s^{n-1}\,cm^{-2}$). As already discussed in literature [17 and references therein], the use of a CPE is required due to a distribution of the relaxation times as a result of inhomogeneities present at the micro or nano (atomic/molecular) level, such as surface roughness/porosity, adsorption, or diffusion. The EEC in Fig. 7 has been used in literature to describe a response of the HER on porous electrodes [26,51,58]. The first time constant (τ_1, $CPE_1 - R_1$) is prescribed to the kinetics of the HER, and it changes (decreases) with overpotential. On the other hand, the second time constant (τ_2, $CPE_2 - R_2$) has been mostly used to describe the porosity of an electrode surface, and hence does not change with overpotential. Therefore, in order to prescribe the two time constants recorded on our Ni/PPY electrodes to specific physical properties, we should first examine their overpotential behavior. Using an equation originally proposed by Brug et al. [61] and later employed by many researchers [8,9,18,25,26,52], $C_{dl,i} = [CPE_i(R_{el}^{-1} + R_i^{-1})^{(1-n)}]^{1/n}$, pure capacitance values (C_{dl}) were calculated from constant-phase element values (CPE) obtained by modeling of EIS spectra, and then the values of the two time constants were calculated knowing that $\tau = R \times C$ (Table 3). A closer inspection of the data in Table 3 shows that the overpotential behavior of the CPE values and corresponding C_{dl} values is potential independent, which indicates that the two CPE elements in the EEC in Fig. 7 represent a response of an electrochemical double layer, i.e. double layer capacitance. CPE (or capacitance) values that change with overpotential do not reflect a response of a double layer, but could be rather associated with hydrogen adsorption processes [17,27,58,59]. Table 3 also shows that an exponent of the first constant-phase element, n_1, is equal to unity, the value that characterizes pure capacitance. On the other hand, values of exponent n_2 are around 0.75, indicating that the CPE_2 is related to a response of a highly non-homogeneous part of the catalyst's surface. The EEC data in Table 3 further demonstrate that with an increase in overpotential both R_1 and R_2 decrease. In addition, the observed overpotential dependence of the corresponding time constant values, τ_1 and τ_2, is exponential (Fig. 7). On a semi-logarithmic plot presented in Fig. 7, both time constants decrease linearly with an increase in overpotential. However, a deviation from linearity is observed at overpotentials below −0.35 V, which is in accordance with the deviations noticed in dc measurements in Fig. 2, which was prescribed to the accumulation of produced hydrogen inside the PPY matrix at the Ni/PPY interface. The observed exponential dependence of time constants on overpotential (Fig. 7) is in accordance with the theory of electron transfer [50], and is thus quite consistent with an overpotential behavior expected for a time constant that describes a response of the HER kinetics. The corresponding slopes of the linear lines are 177 mV decade^{-1} for the first time constant and 198 mV decade^{-1} for the second time constant. These values are somewhat higher than the corresponding Tafel slope values for the same catalyst (138 mV decade^{-1}), but are in the range expected for the HER kinetics, with the Volmer step as a rds. In addition, the value of exponent n_2 and relative ratio of τ_1/τ_2 indicate that the second time constant, τ_2, reflects a response of a part of the Ni surface that is in contact with PPY, i.e. a part of the Ni layer embedded in the polymer matrix. Therefore, this analysis allows us to conclude that both time constants of the EEC in Fig. 7 represent a response of the HER kinetics, where the first time constant (τ_1, $CPE_1 - R_1$) represents a response of Ni islands that are directly exposed to the electrolyte, while the second time constant (τ_2, $CPE_2 - R_2$) reflects a response of the Ni/PPY interface in the interior of the PPY matrix. However, the analysis of EIS data showed that this applies only to Ni/PPY electrodes produced at a short (20 min) Ni deposition time and also to co-deposited Ni/PPY electrodes. On the other hand, the situation with Ni/PPY electrodes produced at long Ni deposition times (1 h:40 min) is quite different. While the first time constant (τ_1, $CPE_1 - R_1$) is still related to the HER kinetics, as discussed above, the second time constant (τ_2, $CPE_2 - R_2$) does not change with overpotential (data not shown here). This indicates that the second time constant is in this case related to the electrode surface porosity response, which is in agreement with the usual literature description of the used EEC model [11,52]. This also shows that the Ni layer above the PPY matrix (Fig. 1e) dominates the EIS response when compared to the response of the part embedded into the PPY matrix. The

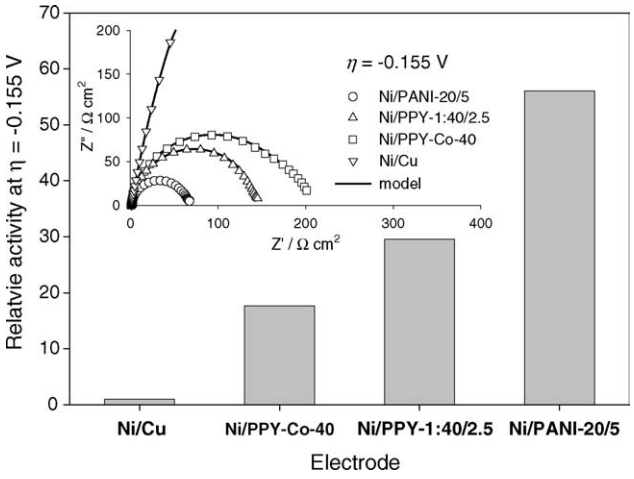

Fig. 8. Relative electrocatalytic activity of the best three Ni/CP catalysts calculated at overpotential −0.155 V. The data were obtained from the EIS results presented in the inset to the figure. A spectrum recorded on a Ni catalysts deposited on Cu substrate (Ni/Cu) is also presented for comparison. Symbols are experimental data and solid lines are modeled data.

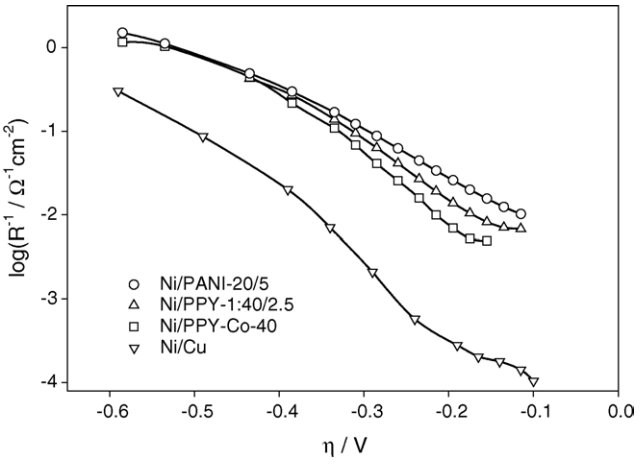

Fig. 9. Tafel curves obtained from the EIS data. *R* represents the charge transfer resistance to the HER.

reason for this could be due to the significant change in the morphology (and surface area available for the HER) of the Ni layer above the PPY matrix, which is quite obvious by comparing the three SEM images presented in Fig. 1d–f.

3.3.2. Ni/PANI electrocatalytic layers

Modeling of EIS spectra obtained on Ni/PANI catalysts using the EEC presented in Fig. 7 resulted in a large error. However, when a one-time constant EEC was used, $R_{el}(CPE_1 - R_1)$, an agreement between the model and experimental data was excellent. An overpotential-dependent behavior of this time constant revealed that its physical meaning reflects the response of the HER kinetics. Considering the large difference in morphology between the Ni/PPY (Fig. 1d–f) and Ni/PANI (Fig. 1g) layers, and taking into account the previous discussion related to the physical meaning of the two time constants recorded on Ni/PPY layers, it is quite reasonable to expect the absence of the second time constant in the EIS response of Ni/PANI layers. Fig. 1g shows that Ni/PANI layer is highly porous, and represents a layer composed of only spherical Ni particles, with only traces of PANI left attached. Thus, the absence of the Ni/PANI interface should also be confirmed by the absence of the second time constant in the EEC, which was indeed evidenced by modeling of Ni/PANI EIS spectra.

The above analysis of EIS data recorded on Ni/CP layers and their comparison with the SEM data shows that the EIS is a very powerful technique that could be used to identify surface/interface processes involved in the HER, obtain the information on the spatial distribution of those processes and on the structure/morphology of the catalyst/polymer/electrolyte interface.

3.3.3. Relative comparison of Ni/PPY and Ni/PANI electrocatalytic layers

Inset to Fig. 8 shows EIS spectra of the three best Ni/CP catalysts, together with a Ni catalyst (control) deposited on a flat Cu substrate. The trend observed is quite similar to the dc trend presented in Fig. 5. The plot demonstrates that the best catalyst is Ni/PANI-20/5, which gives an EIS response characterized by the smallest semicircle (i.e. lowest charge transfer resistance), while Ni/PPY-1:40/2.5 and Ni/PPY-Co-40 show somewhat lower electrocatalytic activity. The control catalyst (Ni/Cu) yields the highest charge transfer resistance (largest semicircle), but due to clarity this spectrum is not fully presented in the figure, but only the rising part of the semicircle. Taking into account that charge transfer resistance is inversely proportional to current (i.e. hydrogen production rate), charge transfer resistance values calculated at −0.155 V (overpotential relevant for the operation of a hydrogen generator) were normalized with respect to the value obtained with the control catalyst (Ni/Cu). This gives qualitative information on the relative catalytic efficiency of the studied composite catalysts and the results are presented on the main plot in Fig. 8. The trend observed reflect the trend seen in Fig. 5. The results demonstrate that Ni/PANI-20/5 catalyst is almost 60 times more active in hydrogen production than the control catalyst, which is due to a large difference in the surface area available for the hydrogen evolution reaction. This is also clearly visible on the SEM images in Fig. 1.

This analysis of the EIS data at a fixed overpotential value could be extended to the whole overpotential range studied. Then, by plotting the logarithm of the inverse of charge transfer resistance, $\log(R_1 + R_2)^{-1}$, versus applied overpotential, η, a Tafelian behavior similar to that in Fig. 5 should be observed. Fig. 9, which shows a set of quazi-Tafel curves obtained from EIS spectra, demonstrates that the observed trend is very similar to the trend expressed by dc polarization measurements in Fig. 5. The corresponding slopes of the Tafel lines calculated from the EIS data in Fig. 9 are presented in Table 4. The obtained values are close to the values calculated from the dc measurements (Table 2), and confirm that the Volmer step (adsorption of hydrogen to form Ni–H_{ads}) is the rate determining step in the hydrogen evolution reaction on all the composite Ni/CP catalysts studied.

Table 4
Tafel slopes calculated from the data presented in Fig. 9

Electrode	b (mV decade^{-1})
Ni/PANI-20/2.5	174
Ni/PPY-1:40/2.5	140
Ni/PPY-Co-40	120
Ni/Cu	131

4. Conclusions

It was shown that pattering of a glassy carbon electrode surface with 3D conducting polymer layers, PPY and PANI, is a convenient method that can be used to increase the surface area of electrodeposited nickel. The influence of a CP layer (matrix) thickness (i.e. CP deposition time) and Ni loading (i.e. Ni deposition time) on the overall electrocatalytic activity of produced electrodes was investigated in the hydrogen evolution reaction. It was demonstrated that all the investigated composite 3D Ni/CP layers offer significantly higher electrocatalytic activity than a Ni layer electrodeposited on a 2D copper substrate. This was explained on the basis of an increased surface roughness (area) of Ni in the composite Ni/CP layer.

The results demonstrate that morphology of the electrodeposited CP matrix has a great influence on the resulting Ni/CP layer morphology, and thus on the overall electrocatalytic activity of the catalyst. PANI matrix, which offers a significantly higher porosity than PPY matrix, enabled a higher Ni surface area (per amount of Ni loaded) to be obtained. The overall best catalytic activity was demonstrated by a Ni/PANI layer formed by incorporating small amounts of Ni into a thick pre-deposited PANI layer. The resulting porous layer, composed of 3 μm interconnected spherical Ni particles, expressed a high tolerance to accumulation of molecular hydrogen in the whole potential region studied.

The electrocatalytic activity of Ni/PPY layers depended greatly on the preparation method used and also on the loading of both PPY and Ni. The highest HER activity within the Ni/PPY group yielded a catalyst prepared by loading a thin and porous pre-deposited PPY layer with larger amounts of Ni (long Ni deposition time). On the other hand, the layer prepared by loading small amounts of Ni inside a thick pre-deposited PPY layer showed the lowest electrocatalytic activity. It was also shown that the co-deposition method offered a significant increase in Ni island dispersion and density, and an island diameter reduction. Two surface regions of Ni in the Ni/PPY layer were found to be active towards HER: Ni islands directly exposed to the electrolyte solution (first region), connected to the GC substrate through Ni 'stalks' embedded into a PPY matrix (second region). It was postulated that the accumulation of hydrogen at the Ni/PPY interface in the interior of the Ni/PPY layer is responsible for the decrease in the HER rate at high overpotentials.

It was found that the rate determining step in the hydrogen evolution reaction on all the catalysts studied is the Volmer step, which involves adsorption of hydrogen to form a Ni–H_{ads} bond. A small electronic influence of the CP matrix on the intrinsic activity of Ni was found.

Acknowledgements

Grateful acknowledgment is made to the Natural Science and Engineering Research Council of Canada and Fonds québécois de la recherche sur la nature et les technologies for support of this research.

References

[1] S. Dun, Int. J. Hydrogen Energy 27 (2002) 235.
[2] T. Hijikata, Int. J. Hydrogen Energy 27 (2002) 115.
[3] P. Kruger, Int. J. Hydrogen Energy 25 (2000) 395.
[4] C. Mitsugi, A. Harumi, F. Kenzo, Int. J. Hydrogen Energy 23 (1998) 159.
[5] M. Kondoh, N. Yokoyama, C. Inazumi, S. Maezawa, N. Fujiwara, Y. Nishimura, K. Oguro, H. Takenaka, J. New Mat. Electrochem. Sys. 3 (2000) 61.
[6] P. Millet, F. Andolfatto, R. Durand, Int. J. Hydrogen Energy 21 (1996) 87.
[7] J. Linnemann, R. Steinberger-Wilckens, 207th Meeting of the Electrochemical Society, Quebec City, Que., Canada, 2005.
[8] P. Los, A. Rami, A. Lasia, J. Appl. Electrochem. 23 (1993) 135.
[9] C. Hitz, A. Lasia, J. Electroanal. Chem. 500 (2001) 213.
[10] S. Tanaka, N. Hirose, T. Tanaki, Int. J. Hydrogen Energy 25 (2000) 481.
[11] W. Hu, Int. J. Hydrogen Energy 25 (2000) 111.
[12] M.H. Miles, M.A. Thomason, J. Electrochem. Soc. 123 (1976) 1459.
[13] B.E. Conway, J.O'M. Bockris, J. Chem. Phys. 26 (1957) 532.
[14] L.I. Krishtalik, in: P. Delahay, C. Tobias (Eds.), Advances in Electrochemistry and Electrochemical Engineering, vol. 7, Interscience, New York, 1970.
[15] S. Trasatti, J. Electroanal. Chem. 39 (1972) 163.
[16] S. Trasatti, J. Chem. Soc. Faraday Trans. 68 (1972) 229.
[17] E. Navarro-Flores, Z. Chong, S. Omanovic, J. Mol. Catal. A: Chem. 226 (2005) 179.
[18] L. Chen, A. Lasia, J. Electrochem. Soc. 138 (1991) 3321.
[19] B.E. Conway, G. Jerkiewicz, Electrochim. Acta 45 (2000) 4075.
[20] J.G. Highfield, E. Claude, K. Oguro, Electrochim. Acta 44 (1999) 2805.
[21] H. Ezaki, M. Morinaga, S. Watanabe, Electrochim. Acta 38 (1993) 557.
[22] H. Ezaki, M. Morinaga, S. Watanabe, J. Saito, Electrochim. Acta 39 (1994) 1769.
[23] H. Shibutani, T. Higashijima, H. Ezaki, M. Morinaga, K. Kikuchi, Electrochim. Acta 43 (1998) 3235.
[24] M. Metikos-Hukovic, A. Jukic, Electrochim. Acta 45 (2000) 4159.
[25] R.K. Shervedani, A. Lasia, J. Appl. Electrochem. 29 (1999) 979.
[26] B. Losiewicz, A. Budniok, E. Rowinski, E. Lagiewka, A. Lasia, Int. J. Hydrogen Energy 29 (2004) 145.
[27] R. Simpraga, G. Tremiliosi-Filho, S.Y. Qian, B.E. Conway, J. Electroanal. Chem. 424 (1997) 141.
[28] H. Ezaki, T. Nambu, M. Morinaga, M. Udaka, K. Kawasaki, Int. J. Hydrogen Energy 21 (1996) 877.
[29] S. Tanaka, N. Hirose, T. Tanaki, Int. J. Hydrogen Energy 25 (2000) 481.
[30] M.M. Jaksic, Electrochim. Acta 45 (2000) 4085;
M.M. Jaksic, Solid State Ionics 136–137 (2000) 733.
[31] R.K. Shervedani, A. Lasia, J. Electrochem. Soc. 144 (1997) 2652.
[32] W. Hu, Int. J. Hydrogen Energy 25 (2000) 111.
[33] P. Dabo, L. Brossard, H. Ménard, P. Tremblay, J. Appl. Electrochem. 28 (1998) 601.
[34] K. Bouzek, K.-M. Mangold, K. Jüttner, Electrochim. Acta 46 (2000) 661.
[35] K. Bouzek, K.-M. Mangold, K. Jüttner, J. Appl. Electrochem. 31 (2001) 501.
[36] H. Laborde, J.-M. Leger, C. Lamy, J. Appl. Electrochem. 24 (1994) 1019.
[37] W.T. Napporn, H. Laborde, J.-M. Leger, C. Lamy, J. Electroanal. Chem. 404 (1996) 153.

[38] M.J. Croissant, T. Napporn, J.-M. Leger, C. Lamy, Electrochim. Acta 43 (1998) 2447.
[39] P.J. Kulesza, M. Matczak, A. Wolkiewicz, B. Grzybowska, M. Galkowski, M.A. Malik, A. Wieckowski, Electrochim. Acta 44 (1999) 2131.
[40] A. Zouaoui, O. Stéphan, A. Ourari, J.-C. Moutet, Electrochim. Acta 46 (2000) 49.
[41] M.T. Giacomini, E.A. Ticianelli, J. McBreen, M. Balasubramanian, J. Electrochem. Soc. 148 (2001) 323.
[42] C. Coutanceau, J.J. Croissant, T. Napporn, C. Lamy, Electrochim. Acta 46 (2000) 579.
[43] C.C. Chen, C.S.C. Bose, K. Rajeshwar, J. Electroanal. Chem. 350 (1993) 161.
[44] L. Torsi, M. Pezzuto, P. Siciliano, R. Rella, L. Sabbatini, L. Valli, P.G. Zambonin, Sens. Actuators B 48 (1998) 362.
[45] A. Jukic, M. Metikos-Hukovic, Electrochim. Acta 48 (2003) 3929.
[46] M. Grzeszczuk, P. Poks, Electrochim. Acta 45 (2000) 4171.
[47] M.M. Saleh, J. Appl. Electrochem. 30 (2000) 939.
[48] L.M. Abrantes, J.P. Correia, Electrochim. Acta (2000) 4179.
[49] B. Pfeiffer, A. Thyssen, J.W. Schultze, J. Electroanal. Chem. 260 (1989) 393.
[50] Southampton Electrochemistry Group, Instrumental Methods in Electrochemistry, Wiley, New York, 1985.
[51] B. Borresen, G. Hagen, R. Tunold, Electrochim. Acta 47 (2002) 1819.
[52] E. Ndzebet, O. Savadogo, Int. J. Hydrogen Energy 20 (1995) 635.
[53] A. Krolikowski, A. Wiecko, Electrochim. Acta 47 (2002) 2065.
[54] V. Tsakova, S. Winkels, J.W. Schultze, J. Electroanal. Chem. 500 (2001) 574.
[55] D.K. Sarkar, X.J. Zhou, A. Tannous, M. Louie, K.T. Leung, Solid State Commun. 125 (2003) 365.
[56] R.J. Nichols, D. Schröer, H. Meyer, Electrochim. Acta 40 (1995) 1479.
[57] M. Hepel, J. Electrochem. Soc. 145 (1998) 124.
[58] L. Birry, A. Lasia, J. Appl. Electrochem. 34 (2004) 735.
[59] E.B. Castro, M.J. de Giz, E.R. Gonzalez, J.R. Vilche, Electrochim. Acta 42 (1997) 951.
[60] B.A. Boukamp, Equivalent Circuit Users Manual, Report CT88/265/128, University of Twente, Department of Chemical Technology, The Netherlands, 1989.
[61] G.J. Brug, A.L.G. Van Der Eeden, M. Sluyters-Rehbach, J.H. Sluyters, J. Electroanal. Chem. 176 (1984) 275.